Measurement and Simulation of Low Carbon Steel Alloy Deposit Temperature in plasma Arc Welding Additive Manufacturing

Abdullah Alhuzaim
Jubail Technical Institute, Jubail Industrial City, 31961, Saudi Arabia
Alhuzaim_af@jti.edu.sa, +966-50433-4699

R. Bruce Madigan
Montana Tech of The University of Montana, Butte, MT 59701 USA bmadigan@mtech.edu, +1406-496-4576

Abstract

Additive manufacturing has the potential to produce near-net shape parts directly from weld metal. Prior work has proved that it is possible to directly manufacture components with complex geometric features and with good productivity. However, under high productivity conditions, deposit temperature increases to a level that it is no longer possible to develop appropriate deposit microstructure and therefore mechanical properties. In this study, Plasma Arc welding was used to produce experimental deposits of 1018 low carbon steel under various conditions. An analytical heat flow model was developed to study the influence of interlayer wait time on deposit temperature and therefore grain size and hardness. The results of the model indicated that as wall height increased, the rate of deposit heat removal by conduction to the substrate decreased leading to a higher preheat temperature after a fixed interlayer wait time causing grain size to increase as wall height increased. However, the model results also show that as wall height increased, the deposit surface area from which heat energy is lost via convection and radiation increased. The model also demonstrated that the use of a means of forced convection to rapidly remove heat from the deposit could be an effective way to boost productivity and maintain smaller grain size and therefore higher hardness and strength in the deposit.

Keywords: Additive Manufacturing, Direct Manufacturing, Free from Fabrication, Metal Deposit, Plasma Arc Welding, Shot Form Feedstock Delivery.

Introduction

The concept of directly manufacturing a component completely out of weld metal has been a possibility for nearly 25 years (Ref.1,2). Additive manufacturing offers the potential to save significant amounts of energy and resources (Ref.3,4) and overcome some limitations of traditional manufacturing methods such as casting, forging and machining. The use of the Plasma Arc welding process for additive manufacturing promises to produce low cost products from vitally important metal alloys (Ref.5). Previous work has demonstrated that it possible to produce relatively complex part shapes and that it is possible to boost metal deposition rate to increase productivity (Ref.6). Attention is now being turned to attaining acceptable mechanical properties and fine geometric features in additively manufactured deposits (Ref.7,8). While the general processing parameters required to produce certain microstructures and hence mechanical properties in low carbon steel alloys are well known, it is difficult to achieve both high productivity and acceptable mechanical properties simultaneously in additively-manufactured. A significant amount of work is being conducted to characterize additive manufacturing process parameters for different alloys. Fusion welding processes like electron beam welding, laser welding, plasma arc welding and gas tungsten arc welding subject the additively manufactured deposit to

repetitive and cumulative thermal cycles that cause complex transformations in steel alloys. The work presented here begins to focus on the next important next step for the PAW process: deposit thermal management to control deposit temperature and therefore microstructure development and resulting mechanical properties.

Investigation Overview

Experimental PAW deposits of alloy 1018 were made under various conditions. A simple analytical heat flow model was developed to simulate the deposit build process. The model was tuned using experimental data in order to extrapolate and predict deposit temperature over a range of conditions that would be cost prohibitive to investigate experimentally. The influence of a limited range of experimental processing conditions on microstructure development was revealed by metallographic observations. The results of the model form the basis on which to develop a strategy to manage deposit heat flow in order to simultaneously improve productivity and obtain acceptable microstructure and mechanical properties.

Experimental Deposit Build Procedure

Linear wall deposits were built on a substrate via Plasma Arc Welding (PAW) with steel shots (Fig. 1).
Both the substrate and shots was Alloy 1018.

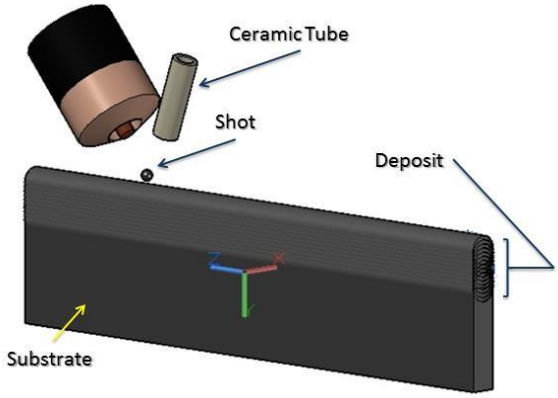

Figure 1: shows the positioning of the PAW torch and shot delivery tube above the substrate prior to welding

The substrate was clamped to a positioning fixture within the Robot the substrate was fixed on the positioner, and the torch standoff distance was set by adjusting the arm torch positioner. The various essential PAW parameters were then set and are shown in the Results and Discussion section for each wall specimen. The essential PAW parameter ranges used to manufacture the weld metal specimens for the additive manufacturing processes are given in Table 1 (Fig. 2). Welding parameters are detailed in Appendix A.

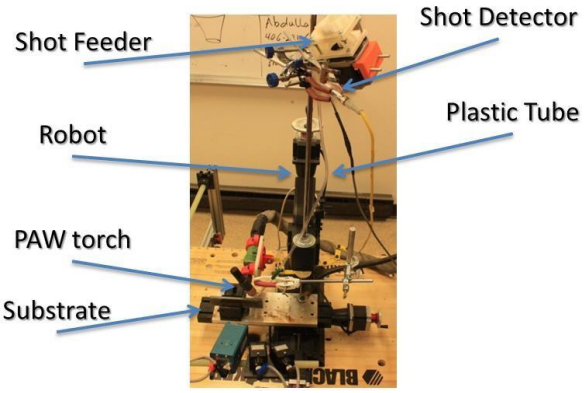

Figure 2: Experimental setup design with shot feeder

Deposit walls were built by placing individual weld layers were placed one atop the previous layer (Fig. 3). The time to complete one individual weld layer, t_t, is determined from the wall length, l_t. The time from the start of one weld layers to the next is the sum of the weld layers deposit time, t_t, and the intertrack wait time t_t . That is, for a given deposit, the inter-track wait time was proportional to the weld track time via . The inter-track wait time allowed cooling of the deposit between weld tracks. was the primary experimental means to control deposit temperature, TD, and therefore to control weld track cooling rate and microstructure development.

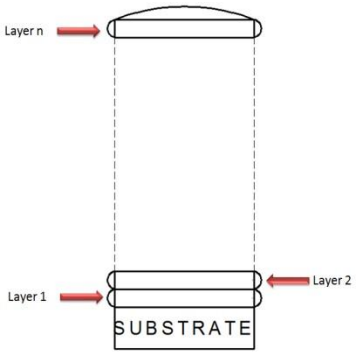

Figure 3: Idealized weld metal deposit build progression

Metallography of Weld Metal Specimen

The waiting time between layers was 1 minute. The PAW essential process parameters used to manufacture the Specimen are shown in Table 1 (Appendix A). Specimen was built using 1018 steel.

The substrate was 150 mm long by 32 mm high and 6.5mm thick. The Specimen was 26 layers producing a deposit 100 mm long by 17 mm high and 7 mm thick. Layer deposition always started from the same end. After each layer, the deposit height was remeasured. The specimen was allowed one minute to cool down between layers.

The deposit grains size change from a relatively small grain size near the substrate to a very coarse microstructure with a large grain size near the tip of the deposit. Figure 4 shows the specimen grains change.

The microstructure of the specimen near the substrate consisted of pearlite colonies (dark contrast) and ferrite grains (light contrast). Both ferrite and pearlite grains were nearly equiaxed grains, ranging from 25 to 50 µm in size.

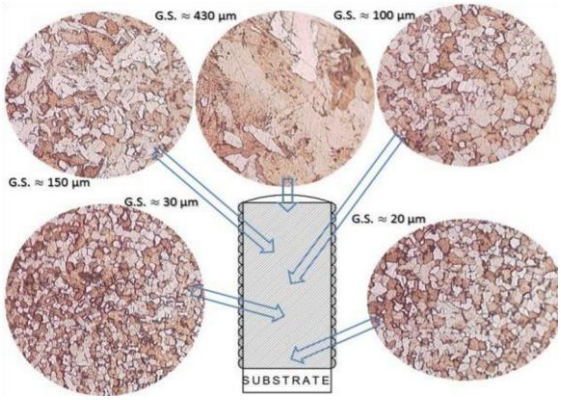

Figure 4: Transverse macro section of the specimen with example micrographs and grain size at deposit heights

The microstructure of the specimen near the surface, the light-colored region of the microstructure, is the ferrite. The grain boundaries between the ferrite grains can be seen quite clearly. The dark regions are the pearlite. It is made up from a fine mixture of ferrite and iron carbide, which can be seen as a "wormy" texture. Both ferrite and pearlite grains were columnar grains which are long, thin, coarse grains, ranging from 300 to 430 µm in size.

Analytical Deposit Model Development

A simple analytical heat flow model, developed (Ref.9) was used to simulate the deposit build temperature T_{dep} in previous work (Ref.10). That model was modified to suit the experimental parameters used in this work. The results of the analytical heat flow model provide the foundation on which to develop a strategy to manage deposit heat flow.

For many heat transfer problems, the first law of thermodynamics provides a useful, often essential tool for heat flow analysis. The conservation of energy for a control volume is given as (Ref.11):

$$\Delta E_{st} = E_{in} - E_{out} + E_g \quad \textbf{Eq1}$$

Since no mechanical work is performed on the control volume, and no energy is generated within the control volume, only thermal energy is considered.
Equation 1 can be rewritten as (Ref.10):

$$Q_{dep} = Q_{weld} - (Q_{cond} + Q_{conv} + Q_{rad}) \quad \textbf{Eq2}$$ Mass, surface area and heat are added to the deposit with each successive weld layer. The model is designed for general methods of layers-based additive manufacturing. A layer can be produced from multiple tracks laid side-by-side as shown in Figure 5 (A) or can be produced from a single track as shown if Figure 5 (B)

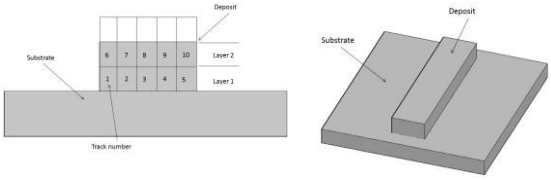

(A) (B)

Figure 5: (A) shown A layer can be produced from multiple tracks laid side-by-side (B) shown a Layer can be produced from a single track.

The cumulative weld metal deposit mass increases as the manufacturing of the deposit increases according to (Ref.10):

$$m_{dep} = m_o + \sum_{n_l=1}^{N_l}\left(\sum_{n_t=1}^{N_t}\Delta m_t\right) \qquad \textbf{Eq3}$$

The cumulative weld metal deposit area similarly increases as (Ref.10).

$$A_{dep} = A_o + \sum_{n_l=1}^{N_l}\left(\sum_{n_t=1}^{N_t}\Delta A_t\right) \qquad \textbf{Eq4}$$

The deposit thermal energy gained via PAW for each weld track is given by:

$$Q_{weld} = \lambda.\eta.E_{avg}.I_{avg}.t_l \qquad \textbf{Eq5}$$

The term λ has physical significance in that it can represent PAW heat transfer efficiency and accounts for heat losses during energy transfer from the arc to the deposit.

In this work, the arc was pulsed from a background level to peak level and back to the background level for each shot delivered to the deposit. Thus each
layer required multiple current pulse cycles such that

$$t_t = n_p\left(t_p + t_B\right) \qquad \textbf{Eq6}$$

To account for arc current pulsing equation 5 is written as

$$Q_{weld} = (I_B.E_B.t_B + I_P.E_p.t_p)\cdot\lambda.n_p \qquad \textbf{Eq7}$$

To simplify the model solution, heat is the considered only to be lost while the arc is off during the interlayer wait-time δt_t. Heat is lost via radiation according to:

$$Q_{rad} = \psi\sigma\varepsilon A_{dep}(T_{dep}^4 - T_{sur}^4)(\delta t_t) \qquad \textbf{Eq8}$$

The term ψ is the scale factor to modify the magnitude of heat lost from the deposit due to radiation. The term ψ has physical significance and can be used as modification of the surface area of the deposit, and/or variations of ε as deposit temperature changes and/or changes in the temperature of the surroundings.

Heat loss by conduction occurred out the sides and bottom of the substrate into the fixture. Heat is lost via conduction according to:

$$Q_{cond} = \xi h_{cond} A_{contact} (T_{dep} - T_{sur})(\delta t_t) \quad \textbf{Eq9}$$

The term ξ has physical significance and can be used as modification of the contact area between the substrate and the fixture, and/or the conduction heat transfer coefficient between the substrate and the fixture, and/or changing the temperature of the fixture in contact with the substrate. Heat lost from the deposit via convection occurs according to (Ref.11):

$$Q_{conv} = \zeta h_{conv} A_{dep} (T_{dep} - T_{\mathrm{sur}})(\delta t_t) \quad \textbf{Eq10}$$

Analytical Heat Flow Model Solution

The analytical heat flow model is solved for the deposit temperature, T_{dep}, as a function of the number of weld tracks, n_t, in the weld metal deposit. The amount of heat accumulated in the weld metal deposit at any instant can be expressed as:

$$Q_{dep} = m_{dep} c_p (T_{dep} - T_{sur}) \quad \textbf{Eq11}$$

If the right-hand-side of Equation 11 for $Q_{dep}$is substituted into Equation 2, the result becomes:

$$m_{dep} C_p = \left(T_{dep} - T_{sur}\right) = Q_{weld} - (Q_{cond} + Q_{conv} + Q_{rad}) \quad \textbf{Eq12}$$

Solving Equation 12 for Tdep results in:

$$T_{dep} = \frac{Q_{weld} - (Q_{cond} + Q_{conv} + Q_{rad})}{m_{dep} c_p} + T_{sur} \quad \textbf{Eq13}$$

and by recognizing that Q_{weld}, Q_{cond}, Q_{conv}, Q_{rad}, and $m_{dep}$are functions of time and, therefore, weld track number, n_t, the weld metal deposit temperature, T_{dep}, can be expressed as:

$$T_{dep}(n_t) = \frac{Q_{weld}(t_l) - [Q_{cond}(\delta t_t) + Q_{conv}(\delta t_t) + Q_{rad}(\delta t_t)]}{m_{dep}(n_t) c_p} + T_{dep}(n_{t-1}) \quad \textbf{Eq14}$$

Where

$$t_t = n_p (t_p + t_B) \quad \textbf{Eq15}$$

Analytical Heat Flow Model Assumptions and Solution Approach

Several assumptions are used to simplify the analytical heat flow model. First, the weld metal deposit thermal energy gained via PAW, Q_{weld}, enters the deposit and diffuses evenly throughout the substrate and deposit immediately after the layer is completed. The first assumption infers that the deposit thermal conductivity is large, and deposit diffusion distances are small. Another assumption is that no heat is lost via conduction, convection, and radiation during the time it takes to complete a weld track. Q_{Cond}, Q_{conv}, and Q_{rad} only occur during the inter-track wait time, δt_t. The initial temperature of the substrate and of the fixture that the substrate rests upon is assumed to be the ambient temperature environment (T_{sur}), (Ref.10).

The approach taken to solve the analytical heat flow model on a track-by-track basis is described as follows. Q_{weld} and Δm_t are added to the deposit. As a result of the newly added mass and heat, an intermediate weld metal deposit surface temperature, Ti, is calculated. ΔA_t is added to the deposit, and Q_{Cond} Q, $_{conv}$, and Q_{rad} are removed from the deposit at the intermediate. As a result of the newly lost heat, the deposit temperature, T_{dep}, is calculated and becomes the starting deposit temperature for the next weld track. Iterations continue for the specified number of weld metal deposit layers.

Results and Discussion of the Analytical

Heat Flow Model

The result of the analytical heat flow model is T_{dep} as a function of t_t n_t, λ, ψ, ξ, and ζ. The coefficients λ, ψ, ξ, and ζ were adjusted to allow the analytical heat flow model deposit temperature to approximate the experimental measured deposit temperature. two δt_t values were used, the actual specimen was $\delta t_t 1min$ = 60 sec and hypothetical value of δt_t= 10 sec. The model is capable of predicting T_{dep} (nt) for an unlimited number of layers, however in this research, n_t was limited to be 200 layers. The analytical heat flow model was solved by using a spreadsheet computer program. Analytical heat flow model properties for low-carbon steel, along with their typical values, are also shown in (Ref.15). The analytical heat flow model properties and mathematical formulas were taken from Refs.
(Ref.12), (Ref.13) and (Ref.14).

Deposit mass, surface area and heat input increase linearly with n_t. Increased mass causes the deposit to contain more thermal energy, while increased surface area allows the deposit to shed more thermal energy via radiation and convection. Increased deposit height reduced the amount of heat loss to the fixture via conduction. A maximum T_{dep} was selected for a steel deposit based on the Fe-C phase diagram. Ideally, T_{dep} would stay below the eutectoid temperature approximately 2 Lower temperature reduces grain growth and produces a refined microstructure in the deposit, both of which lead to better mechanical properties.

As mentioned the scale factors, λ, ψ, ξ, and ζ were adjusted to match the model simulated deposit temperature to the experimental deposit temperature. Figure 6 shows experimental and simulation T_{dep} as a function of n_t. The experimental deposit temperature measurements are shown in Tables 25 and 26 the values for the model scale factors λ, ψ, ξ, and ζ used in Figure 6

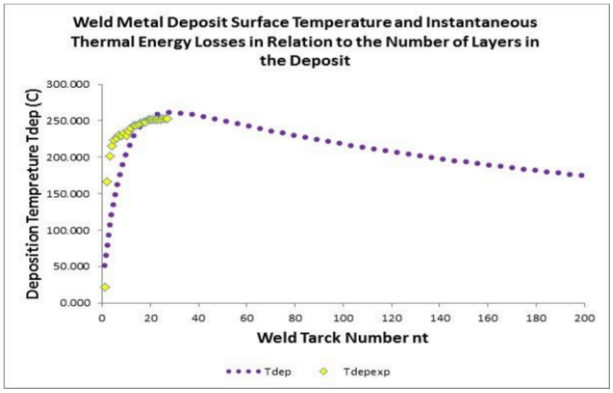

Figure 6: Experimental and Simulation as a function of nt

Since the model shows very close results from the beginning of the building to 26 layers, a prediction can be made from the graph. For this solution to the analytical heat flow model, δt_t = 1 minute (60 seconds), which is the same δt_t that was used to manufacture the specimen. Other property values used to solve the analytical heat flow model are shown in (Ref.15). The values of λ, ξ, ψ, and ζ, are listed in Table 2.This allows the model temperatures to predict the approximation of the experimental temperatures. Since the model shows very close results from the beginning of the building to 26
layers, a prediction can be made from the graph

The model was tuned using the perimeter reasonably match the experimental deposit temperature. In Figure 7, the total number of experimental temperature reading results is limited to the experimental range of layers (≈ 26).With the values of δ (0.28) T_{dep} increases to a peak value of approximately 200 °C after 26 layers. T_{dep} begins to decrease slightly after each individual layer as predicted by the model.
The conditions used to obtain the solution to the analytical heat flow model for the specimen shown in Figure 6 represent a condition of high heat loss via conduction. Conduction is the dominant heat loss mechanism for the prescribed conditions, as the number of layer increases the heat loss via conduction decrease. The amount

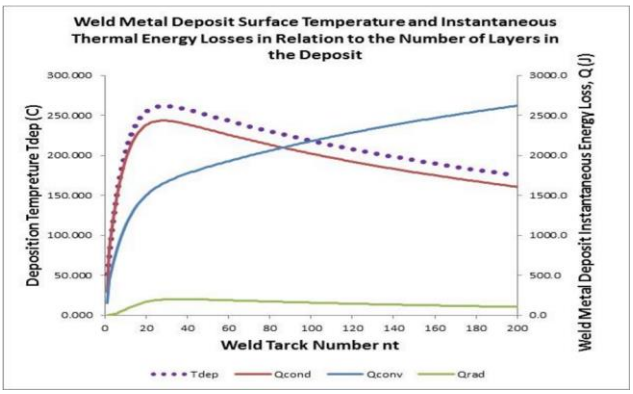

Figure 7: Experimental and Simulation as a function of nt for $\delta tt = 60$ seconds

of heat loss by conduction is depending on the temperature deposited and the distance of the heat have to travel through the specimen to the fixture is linear with deposit height and deposit temperature. As the height of the deposit increases the heat loss by conduction decreases, for two reasons; the temperature of the deposit decreases and the height of the deposit increase.

An increased in heat lost via convection to be the dominate heat loss with increase in number of layers. Convection accounts for most thermal energy losses as the area increases. The curve of the heat loss via convection can be understood better with referral to equation (10). Heat loss via radiation is the lower heat loss, although increase in area is a direct factor to increase in heat loss via radiation. However, the reduction in temperature deposited has more effect since the temperature in Q_{rad} is raised to the power 4 (see equation 8). All of the heat transfer mechanisms increase with increasingn_l to a certain level and approach a maximum value, and then start to decrease except convection as a result of the increasingA_{dep}.

T_{dep} generally increases as more weld metal layers are deposited when n_l is small. When n_l is small, T_{dep} increases linearly. As more weld layers are deposited, the rate at which T_{dep} increases begins to decrease. After certain A_{dep} is reached, T_{dep} reaches a maximum value and begins to decrease as a result of the combined effects of thermal energy losses resulting from conduction, convection, and radiation. The values used to develop Figure 8 are displayed in Table 2 (located in Appendix A).

The analytical heat flow model shown in Figure 8 demonstrated that higher maximum values of T_{dep}can be achieved by decreasing δt_t to 10 second. This is a relatively small value of δt_t ,which is effective at increasing productivity. Productivity can be boost at the expense of mechanical properties. A plot of the simulation T_{dep} developed from the analytical heat flow model for n_t= 200 is shown in Figure 7.

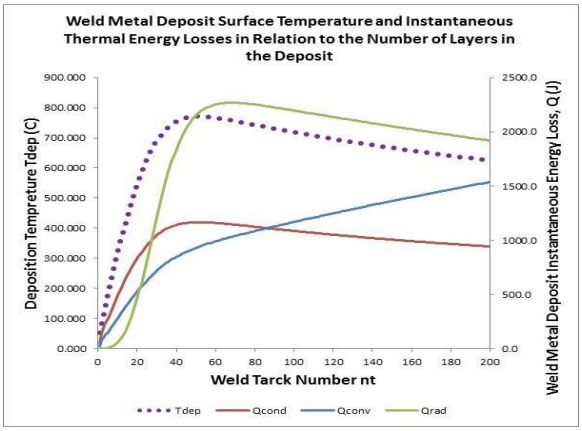

Figure 8: Experimental and Simulation T_{dep}as a function of nt for δtt = 10 seconds

The wait time was decrease more than 6 times from the calibrated model. The heat transfer mechanisms did not behave the same as δt_t = 1 minute (60 Sec.). The conditions used to obtain the solution to the analytical heat flow model for shorter inter-layer wait-time in Figure 8 represent a condition of high heat loss via Radiation. The increase in temperature deposited has direct effect in Q_{rad}since the temperature in Q_{rad} is raised to the power 4 (see equation 8). Conduction also, increases to a peak level then as the number of layer increases the heat loss via conduction decrease. Thermal energy loss via convection increase linearly as the area increases.

T_{dep} is greater comparing to δt_t = 1 minute (60 Sec.). Generally, increases as more weld metal layers are deposited when n_l is small. When n_l is small, T_{dep} increases. As more weld layers are deposited, the rate at which T_{dep} begins to decrease linearly. After certain A_{dep} is reached, T_{dep} reaches a maximum value and begins to decrease as a result of the combined effects of thermal energy losses resulting from conduction, convection, and radiation. The values used to develop Figure 8 are displayed in Table 2 (located in Appendix A).

Higher values of T_{dep} increase grain growth and produce columnar grains which are long, thin, coarse grains microstructure in the deposit. Poorer mechanical properties are achieved as a result of increase in grain growth and coarse microstructures in the weld metal deposit. T_{dep} reaches the mild steel eutectoid temperature in the Fe-C phase diagram (about 727 C) which will lead to eutectoid transformation to produce ferrite and cementite. The possibility of improving thermal energy flow from the weld metal deposit is demonstrated by the analytical heat flow model. Improving heat flow from the deposit controls the weld metal microstructure while simultaneously maintaining high productivity. An important step in the advancement of AM techniques is thermal management of the weld metal deposit. Thermal management of the weld metal deposit controls the deposit temperature and, therefore, microstructure development and the resulting mechanical properties (Ref.10).

Conclusion

An analytical heat flow model was developed to study the influence of interlayer wait time on deposit temperature and therefore grain size and hardness. The results of the model indicated that as wall height increased, the rate of deposit heat removal by conduction to the substrate decreased leading to a higher preheat temperature after a fixed interlayer wait time causing grain size to increase as wall height increased.

The model results also show that as wall height increased, the deposit surface area from which heat energy is lost via convection and radiation increased. The model also demonstrated that the use of a means of forced convection to rapidly remove heat from the deposit could be an effective way to boost productivity and maintain smaller grain size and therefore higher hardness and strength in the deposit.

Acknowledgments

This work was sponsored in-part by the Royal Commission for Jubail and Yanbu under scholarship number (1039/20/6)

References

1. **C.O. Brown, E.M. Breinan and B.H. Kear.** *Method for Fabricating Articles by Sequential Layer Deposition. 4.323.756* U.S. , 1982.
2. **Edmonds, M.D. McAninch and D.P.** *Method and Apparatus for Building a Workpiece by Deposit Welding. 4,775,092.* U.S., 1988.
3. *Electron Beam Freeform Fabrication Fabrication: A Metal Deposition Apparatus to Build Components Directly from CAD.* **Taminger, Karen.** Arlington, Texas : NASA Langley Research Center, March 26-27, 2008. available at technologygateway.nasa.gov/docs/EBF3Overview.pdf.
4. *Electron Beam Freeform Fabrication for Cost Effective Near-Net Shape Manufacturing.* **Hafley, Karen M. Taminger and Robert A.** s.l. : NASA Langley Research Center. Metals & Thermal

Structures Branch. Mail Stop 188A, Hampton, VA 23681-2199 USA available at technologygateway.nasa.gov/docs/20080013538_200 8013396.pdf.

5. *Direct Digital Manufacturing of Metallic Components: Direct Digital Manufacturing of Metallic Components Affordable, Durable, and Structurally Efficient Airframes.* **Frazier, W.E.** at the Holiday Inn, Solomons Island, MD : s.n., 11 - 12 May 2010, Vision and Roadmap.
6. Sciaky Manufacturing. [Online] http://www.sciaky.com/direct_manufacturing.html.
7. *Qualification of Metallic Materials and Structures for Aerospace Applications.* **William Frazier, Don Polakovics, and Wayne Koegel.** March 2001, JOM.
8. *Shaped Metal Deposition of a Nickel Alloy for Aero Engine Applications.* **Clark, D., M. R. Bache, and M. T. Whittaker.** 2008, Journal of Materials Processing Technology 203, pp. 439-448.
9. **Stavinoha, Joe N.** *Investigation Of Plasma Arc Welding As A Method For The Additive Manufacturing Of Ti-6Al-4V Alloy Components.* Butte : Montana Tech, 2012.
10. *Measurement And Simulation Of Titanium Alloy Deposit Temperature In Electron Beam Additive Manufacturing.* **Madigan, R. Bruce, Sean F. Riley, Mark J. Cola, Vivek R. Dave, and John E. Talkington.** Chicago, Illinois : ASM International,, 2012. Ninth International Trends in Welding Research Conference.
11. **Incropera, Frank P., David P. DeWitt, Theodore L. Bergman, and Adrienne S. Lavine.** *Introduction to Heat Transfer.* Fifth ed. Hoboken. New Jersey : John Wiley & Sons, Inc., 2007.
12. **Donachie, Matthew J.** *Titanium Technical Guide.* Second. Materials Park, Ohio : ASM International, 2000.
13. **Messler, Robert W.** *Principles Of Welding: Processes, Physics, Chemistry, And Metallurgy.* s.l. : Weinheim, Baden-Württemberg, Germany: WileyVCH., 2004.
14. **Association, Staff of Research and Education.** *The Handbook of Mechanical Engineering.* Piscataway, New Jersey : Research and Education Association., 2004.
15. **Alhuzaim, Abdullah F.** *INVESTIGATION IN THE USE OF PLASMA ARC WELDING AND ALTERNATIVE FEEDSTOCK DELIVERY METHOD IN ADDITIVE MANUFACTURE.* Butte, MT : Montana Tech of the university of Montana, 2014. Available at http://www.abdullahalhuzaim.com/wpcontent/uploads/2014/05/Additive-Manufacture.pdf

Appendix A

Table 1: Essential Variables for PAW

Parameter	Value/Range
Automation Level	Mechanized/Robotic
Electrode Setback	Gauge 1
Orifice Diameter	2.4mm
Shielding Gas	Argon @ 18CFH
Plasma Gas	Argon @ 2CFH
Voltage	Vp = 20V Vb =16V
Amperage	Ip = 50A Ib = 9A

Current Type	DCEN
Tungsten Type/Size/Prep	W+Th,La,Cs / 2.4mm / Pointed with landing
Travel Speed	Actual 22.22mm/min Theoretical 20mm/min
Torch Stand-off	4mm
Filler Material	1018 Steel
Base Material Substrate	A36 Steel
Transfer Mode	Transferred Arc
Welding Mode	Melt-In

Table 2: Properties Used to Solve the Analytical Heat Flow Model

Model Property	Value1
mo (g)	2607.400000
Δmt g	3.280500
Ao (m2)	0.011966
ΔAt m2	-04
cp [J/(g·°C)]	
ε	1.280000E 0.050000 0.500000
ζ [W/ m2·K4]	5.670000E-08
Qweld (J)	11880.0
δtt (s)	60
	50
	13
hcond [W/(m2·K)]	
hconv [W/(m2·K)]	
λ	0.60
ξ	0.50
ζ	0.50
ψ	1.00
Tsur (°C)	22.00

Appendix B

Glossary of Terms Term Definition

A	Ampere
Aarc	Arc area (mm2)
AC	Alternating current
Adep	Cumulative deposit area (in².)
Ain	Inner surface area of deposit (in².)
AM	Additive manufacturing
Ao	Original substrate area (in².)
A36	Plain carbon steel alloy
CAD	Computer-aided design
Cb	Columbium
CC	Constant current
DC	Direct current
DCEN	Direct current electrode negative
DM	Direct manufacturing
Eg	Thermal energy generation in a control volume (J)
Ein	Thermal and mechanical energy entering a control volume (J)
Eout	Thermal and mechanical energy leaving a control volume (J)
FFF	Free-form fabrication
HAZ	Heat-affected zone
hcond	Conduction heat transfer coefficient [*W*/ m2·K]
hconv	Convection heat transfer coefficient [*W*/ m2·K]
hcp	Hexagonal close-packed
hspec1	Specimen 1 height (mm.)
hspec2	Specimen 2 height (mm.)
ht	Weld track height (mm.)
Iarc	Arc current (A)
In.	Inch
J	Joule
K	Kelvin
kg	Kilogram
ksi	1,000 pounds per square inch
lb.	Pound
LM	Layered manufacturing
m	Meter
MD	Metal deposition
mdep	Cumulative deposit mass (kg)
min	Minute
mm	Millimeter
mo	Original substrate mass (kg)
nl	Layer “n” in the deposit
Nl	Number of layers per deposit
nt	Track “n” in the deposit

Nt	Number of tracks per layer
Parc	Arc power (*W*)
PAW	Plasma arc welding
PD	Power density (*W*/mm2)
psi	Pounds per square inch
Q	Deposit thermal energy lost (J)
Qcond	Deposit thermal energy lost via conduction (J)
Qconv	Deposit thermal energy lost via convection (J)
Qdep	Accumulated deposit thermal energy (J)
Qrad	Deposit thermal energy lost via radiation (J)
Qweld	Deposit thermal energy gained via PAW (J)
RM	Rapid manufacturing
RP	Rapid prototyping
s	Second
sl	Substrate length (mm.)
sw	Substrate width (mm.)
sh	Substrate height (mm.)
SMD	Shaped metal deposition
sv	Substrate volume (mm^3)
Tdep	Deposit temperature (°C)
Texp	Experimental deposit surface temperature (°C)
Tfluid	Fluid temperature (°C) (used in Mathcad analytical heat flow model solution)
To	Original deposit surface temperature (°C)
Ts	Deposit temperature (°C) (used in Mathcad analytical heat flow model solution)
tspec	Specimen thickness (mm.)
Tsur	Surrounding/ambient temperature (°C)
tt	Time to weld one track (s)
V	Voltage
W	Tungsten
W	Watt
wt%	Weight percent
δtt	Wait time between weld tracks (min)
Δ*At*	Area added to substrate after each weld track (mm.2)
Δ*Est*	Change in thermal and mechanical energy stored in a control volume (J)
Δ*mt*	Mass added to substrate after each weld track (kg)
ε	Emissivity
ζ	Scale factor to modify the convection heat transfer coefficient
ζhconv	Modified effective convection heat transfer coefficient [*W*/ m2·K]
λ	Scale factor to modify the PAW heat transfer efficiency
η	Modified effective PAW heat transfer efficiency (%)
μm	Micrometer (1 x 10-6 m)
ξ	Scale factor to modify the conduction heat transfer coefficient
ξhcond	Modified effective conduction heat transfer coefficient [*W*/ m2·K]
π	Mathematical constant ≈ 3.14

ρ	Density (g/cm3)
ζ	Stefan-Boltzmann constant [5.67 x 10-8 *W*/ m2·K4]
Σ	Summation
ψ	Scale factor to modify the magnitude of heat lost due to radiation
ζ	Modified effective Stefan-Boltzmann constant [*W*/ m2·K4]